Stable and radioactive carbon isotope partitioning in soils and saturated systems: a reactive transport modeling benchmark study

Jennifer L. Druhan[1]&Sophie Guillon[2]&Manon Lincker2&Bhavna Arora[3]

jdruhan@illinois.edu

Abstract

This benchmark provides the first rigorous test of a three-isotope system [^{12}C,^{13}C, and^{14}C] subject to the combined effects of radioactive decay and both stable equilibrium and kinetic fractionation. We present a series of problems building in complexity based on the cycling of carbon in both organic and inorganic forms. The key components implement (1) equilibrium fractionation between multiple coexisting carbon species as a function of pH, (2) radioactive decay of radiocarbon with associated mass-dependent speciation demonstrating appropriate correction of the$\Delta 14C$ value in agreement with reporting convention, and (3)kinetic stable isotope fractionation due to the oxidation of organic carbon to inorganic forms as a function of time and space in an open, through-flowing system. Participating RTM codes are Crunch Tope, Tough React, Hytec, and The Geochemist's Workbench. Across all problem levels, simulation results from all RTMs demonstrate good agreement.

Keywords

Carbon isotopes

Equilibrium fractionation

Kinetic fractionation

Radioactive decay

Reactive transport

1 Introduction

In recent years, application of multi-component numerical re-active transport models (RTMs) to quantify the partitioning of both stable and radiogenic isotopes has yielded new insight into the (bio)geochemical cycling of elements through marine sediments [1,5,20], secondary mineral growth [8,24], fluid transport and mechanisms of mixing [6,11,23,27], terrestrial weathering rates and mechanisms [21], and contaminant fate and degradation pathways [7,9,10,13,15,16,29]. It is notable that the majority of isotopic applications of numerical RTMs listed above involve carbon as a reaction driver. However, to date, the direct numerical simulation of both organic and inorganic carbon isotopes in multi-component reaction networks remains largely undemonstrated. Furthermore, carbon age and residence time in soils measured using radio-carbon is still largely quantified through

box-model approaches which neglect the complexity of through-flowing, biogeochemically active soils. Carbon cycling in the near-surface environment involves a complex network of reactivity, including equilibrium speciation, redox transitions, biological utilization, and storage in a wide variety of organic and inorganic pools. The stable isotopes of carbon ($\delta^{13}C$) are commonly utilized to disentangle this complexity through the characteristic fractionations associated with both equilibrium and kinetically controlled reactions, resulting in a wide range of applications from paleo proxies to contaminant remediation. From this perspective, the utility of modern RTM techniques in quantifying subsurface carbon fate and transformation has yet to be fully realized [19]. To some extent, this lag may be due to the additional complexity inherent in simulating a system where multiple aqueous species exist in tandem (e.g., $CO_2(aq)$,HCO_3^-,andCO_3^{2-}) each with distinct equilibrium partitioning of the stable isotopes of carbon. In addition to the use of natural stable isotope fractionation factors (α) as a tracer for process, stable carbon isotope partitioning is embedded in the standard set of corrections used to report radiocarbon values, indicating that any mass-dependent partitioning must be tracked in tandem with radio-carbon decay and distribution in order to accurately simulate the evolution and apparent age of radiocarbon across long-lived “recalcitrant” carbon pools. In addition, an increasing number of studies are employing ^{13}C-labeled carbon compounds and even radiocarbon tracers to probe the functioning of microbial populations, quantify contaminant degradation rates, and identify the pathways of carbon mobility in the subsurface. Given such widespread use of natural and labeled stable car-bon isotopes and radiocarbon tracers in the earth sciences, it is necessary for reactive transport codes to accurately and consistently simulate carbon isotope partitioning through both equilibrium and kinetic pathways, as well as reproduce the distribution of labeled carbon compounds bearing ^{13}C signatures and ^{14}C“pulses”that differ from natural values by many orders of magnitude. Notably, the combination of stable isotope partitioning, which occurs on the timescales of instantaneous equilibration to kinetically driven microbial activity, and a radioisotope with a half-life of 5730 years results in a unique multi-isotopic system capable of tracing processes over a broad temporal scale. This presents a unique challenge and opportunity to the reactive transport modeling community, in that the stable isotope signature of a given carbon pool is utilized both as a quantitative measure of microbial activity, degradation rates, and carbon de-composition pathways, and also as a correction factor for mass-dependent fractionation of radiocarbon. Therefore, accurate models of long-term soil carbon composition must track both rapid stable isotope partitioning and long-term radioactive decay while appropriately accounting for mass-dependent partitioning of all isotopes in all compounds and phases. Here, we present a benchmark problem set for reactive trans-port software comprised of four levels, culminating in the simulation of a recent flow-through column study of microbial acetate oxidation in natural sediments containing an artificial ^{13}C label [9,10]. The

problem set is divided into a hierarchical sequence building in complexity to the final component. Part 1 describes a simple equilibrium speciation for the carbonate system featuring appropriate non-unity fractionation factors for δ13C between aqueous compounds as a function of pH. The intention of this exercise is to introduce the partitioning of stable isotopes and provide a benchmark level that is testable against an analytical solution. Part 2 involves a simple timeseries with the introduction of radiocarbon decay. The purpose of this component is to demonstrate that the decay curve is accurately reproduced while simultaneously tracking the associated stable isotope ratio and applying the appropriate correction. Part 3 is subdivided into two sections. The first introduces kinetically controlled microbial oxidation of organic carbon including stable carbon isotopes subject to equilibrium speciation in a batch reactor. The second adds the effects of a 1D flow, sorption, and biogenic mineral formation.

Component problem set 1: Speciation of carbonate system with non-unity equilibrium fractionation factors at a range of pH values

Component problem set 2: Radiocarbon decay with ap-propriate associated stable carbon isotope correction factor

Component problem set 3: Simulation of natural carbon isotope fractionation due to oxidation of an organic car-bon electron donor converted to inorganic carbon, including speciation and microbially mediated kinetics (a) in a batch reactor and (b) in a 1D flow path based on a published column experiment

2 Reactive transport software

2.1 Crunch Tope

This software is an open source multi-component reactive transport code originally developed and maintained by Carl Steefel and colleagues at the Lawrence Berkeley National Laboratory (https://bitbucket.org/crunchflow/crunchtope/wiki/Home). The software has been utilized for a broad variety of near-surface environmental simulations [25] and several isotope-specific modifications have been implement-ed, allowing for a solid solution model to form isotopically fractionated solids from solution [8], and fractionate isotopes through microbially mediated reactions [9,10].

2.2 Tough React

This software is commercially available and is developed and maintained by the Lawrence Berkeley National Laboratory. Itis a full multi-phase simulator and has been applied extensively in the context of geothermal energy and nuclear waste repositories [2]. Several modifications to the code have been made to create the same mineral and microbial isotopic capabilities as Crunch Tope [14,29].

2.3 The Geochemist’s Workbench (GWB)

The Geochemist’s Workbench (GWB) is a commercially available reactive transport simulator that is widely used in both industry and academic research. The code is distributed and maintained by Aqueous Solutions. Several isotope-specific capabilities are implemented [18] which are unique in approach to the rest of the software.

2.4 Hytec/chess

This software is a commercially available multi-component multi-phase reactive transport code originally developed and maintained by MINES Paris Tech, that integrates a wide variety of features and options that have evolved, after more than a decade of development, to a widely used and versatile simulation tool [28]. Several modifications to the code have recently been made to create the same mineral and microbial isotopic capabilities as Crunch Tope.

3 Implementing isotope ratios and fractionation

A complete description of the mathematical framework under-lying flow, transport, and reactivity in the four software pack-ages described above is beyond the scope of the current benchmark and the interested reader is referred to the supporting references as well as Steefel et al. [25]. Here, we describe the implementation of isotopes and their associated partitioning within the context of these reactive transport soft-ware packages. As described in the benchmark components (Section4), each isotopologue of a given compound is introduced in the models as a unique “species.” For example, a primary inorganic carbon species HCO_3^- is simulated using three separate concentrations of $H^{12}CO^-_3$, $H^{13}CO^-_3$,and$H^{14}CO^-_3$, where for natural abundances, the concentration of $H^{13}CO^-_3$will be roughly 1% that of $H^{12}CO^-_3$,and $H^{14}CO^-_3$ will be on the order of parts per trillion (10^{-12})less than $H^{12}CO^-_3$. At this point, the three “species” all sum up to the total concentration of HCO^-_3, but from the perspective of the model implementation, they are completely independent. This means that all associated equilibrium relationships with secondary species have to be incorporated for all three iso-topes. If a given equilibrium, for example, between HCO3−and CO_2(aq)is implemented with precisely the same equilibrium constant (Keq) for all isotopes, then the equilibrium fractionation factor is equal to 1.0, i.e.,$\alpha eq = {}^{13}Keq/{}^{12}Keq = 1.0$.Any fractionation associated with equilibrium partitioning is then entered into the models by changing the rare isotope equilibrium constant relative to the major isotope value to implement the desired αeq. Similarly, any kinetic reaction (see benchmark component set 3 below) must be included for each of the isotopes, and any kinetic fractionation is implemented as a difference between the kinetic rate constants(k), i.e., $\alpha k = {}^{13}k/{}^{12}k$. More complex reaction rate formulations require further consideration (e.g., [9]).

Stable isotope ratios are frequently cast in terms of delta notation, and in the current models, this is easily calculated by taking the ratio of concentration of the rare ^{13}C isotopologue relative to the common ^{12}C counterpart. This

ratio is then normalized relative to a standard value, for carbon typically the vPDB ($^{13}C/^{12}C_{std}$= 0.0112372). Finally, this is converted to per mil units following the formulation:

$$\delta^{13}C = \left(\frac{^{13}C\,/^{12}C_{\text{model}}}{^{13}C\,/^{12}C_{\text{std}}} - 1 \right) \times 1000 \qquad (1)$$

The corresponding radiocarbon notation is similarly reported using standard methods [26]. Critically, in the process of collecting radiocarbon values, the ratio of $^{14}C/^{12}C$ is corrected for any mass-dependent effects using the corresponding $\delta^{13}C$ of the sample (Eq.2). The resulting ratio is then converted to $\Delta^{14}C$ notation using a$^{14}C/^{12}C_{std}$is 1.12E−12. The current year is somewhat arbitrary for the present application, and is taken as 2019 for the purposes of the present paper (Eq.3).

$$^{14}C/^{12}C_{\text{corr}} = \left(^{14}C\,/^{12}C\right)\left(\frac{1+\delta^{13}C_{\text{std}}/1000}{1+\delta^{13}C_{\text{meas}}/1000}\right)^{2} \qquad (2)$$

$$\Delta^{14}C = \left(\frac{^{14}C/^{12}C_{\text{corr}}}{^{14}C/^{12}C_{\text{std}} \times \exp\left(\frac{\text{year}-1950}{8267}\right) - 1} \right) \times 1000 \qquad (3)$$

As described in the introduction, this coupling of mass-dependent stable isotope partitioning and radioactive decay in the$\Delta^{14}C$ notation is ubiquitously employed, but has yet to be rigorously benchmarked in a reactive transport context. Furthermore, we note an interesting feature of the carbon isotope system in that the difference in mass of radiocarbon relative to the common ^{12}C isotope is twice that of the difference between ^{12}C and ^{13}C; thus, the mass-dependent fractionations imposed between all radiocarbon species and the common ^{12}C through their equilibrium constants must be twice that of the fractionation factor between ^{13}C and ^{12}C. This is implemented in all the software packages in the present simulations, and in fact, failure to do so leads to spurious behavior when Eq.2 is applied as the ^{13}C isotope ratio fails to account for the complete partitioning between radiocarbon and ^{12}C. This difference has been noted previously [26] and is highlighted here to emphasize this important check of accuracy.

Finally, implementation of radioactive decay for the ^{14}C isotopologue of any species is easily implemented as a first order kinetic reaction. This is described in further detail in component set 2 (Section4.2). It is important to recognize that in the present simulations, the application of Eqs.2 and

3couples shifts in radiocarbon and stable carbon isotope ratios, but the choice of year (here 2019) is arbitrary for this benchmarking exercise (normally used as a correction since atmospheric bomb pulse). In this benchmark, component sets including radiocarbon are running forward in time from some initial condition and including radioactive decay; thus, the value of $\Delta^{14}C$ should decrease through time at exactly the same rate and value for all carbon species in the system.

4 Detailed problem description

4.1 Component problem set 1: Speciation of carbonate system with non-unity equilibrium

fractionation factors at a range of pH values

Part 1 introduces geochemical parameters appropriate for inorganic carbon speciation with appropriate pH-dependent equilibrium fractionation of $\delta^{13}C$ between car-bon species in solution. The solution contains dissolved inorganic carbon (DIC), split into ^{13}C DIC and ^{12}C DIC subcomponents, resulting in explicit tracking of the $\delta^{13}C$ value, as well as background electrolytes. A gas phase CO_2 component may easily be included in equilibrium with dissolved $CO_2(aq)$, but is omitted here for simplicity. The total DIC is thus a balanced sum of $CO_2(aq)$,HCO^-_3 and CO_3^{2-}in solution. Given that the initial isotope ratio of the total DIC is input into the simulation, and there are no heterogeneous reactions or open system behavior implemented in this simulation, there should be no shift in the $\delta^{13}C$ of total DIC with time. Any alteration to this total concentration ratio would constitute a mass imbalance. However, the equilibrium partitioning between dissolved species comprising DIC is specified using the parameters reported by Mook [22] for a temperature of 25 °C. These non-unity equilibrium fractionation factors result in a distribution in the equilibrated $\delta^{13}C$ isotope ratios across the coexisting dissolved carbonate species $CO_2(aq)$,HCO^-_3, and CO_3^{2-}which is systematically tracked throughout a range of pH from 3.0–13.0 along with the species distribution of total DIC. This relatively simple exercise may be validated against an analytical solution to demonstrate the capacity of a multi-component RTM approach to quantify and predict the distribution of carbon isotope species subject to a suite of coupled chemical equilibria as a function of pH. The same approach may be readily extended to temperature-dependent fractionation factors by implementing a range of non-unity α values as differences in the temperature-dependent equilibrium constants for the isotopes of each species.

4.1.1 Flow and transport model specification

There is no open system behavior included in part 1 and thus no flow model is implemented. The domain is effectively 0D.

4.1.2 Reaction network specification

The simulations are run for six initial conditions, each of which is unique only in the starting pH value.

These are summarized in Table1. The resulting $\delta^{13}C$ of total DIC is then0.97‰ relative to the vPDB standard (0.0112372). The secondary species and associated equilibrium constants at 25 °C are given in Table2.Though not included in the present simulations, we also pro-vide the appropriate equilibria for gas phase CO_2. The slight differences in logK values for each of the rare ^{13}C isotopologues of the individual secondary carbonate species compared with the logK values of the major isotopologues, reflects the equilibrium isotopic fractionation between these species and the primary HCO_3^- at 25 °C as reported by Mook [22].

4.1.3 Runtime parameters

The simulation is restricted to a speciation calculation and thus both CrunchTope and GWB are set to “speciate only” requirement so that no time stepping is activated. ToughReact and Hytec return an output file at the initiation of the run with equilibrates species for all conditions implemented, and is thus run for an arbitrarily short time in order to obtain this file.

4.1.4 Analytical solution

The parameter set provided in Table2 results in a series of equilibrium expressions for the individual carbonate species concentrations and their associated $\delta^{13}C$ as a function of pH.

Table 1 Initial total concentration of the primary aqueous species at 25 °C. All carbon isotopes not explicitly treated as ^{13}C are lumped into the remaining DIC pool, of which the vast majority is ^{12}C

Primary species	Initial concentration (mmol/kg H_2O)
pH	3.0, 5.0, 7.0, 9.0, 11.0, 13.0
DIC (as HCO_3^-)	5.087E−01
DI^{13}C (as H$^{13}CO_3^-$)	5.5502E−03
Na^+	Charge balance
Cl^-	5.0

Table 2 Secondary aqueous and gaseous species with equilibrium constants at 25 °C

Secondary species	Equilibrium constant (log K)	Notation for analytical solution
NaCl	0.7770	
NaOH	14.7948	
HCl	−0.6700	
OH-	13.9951	
$CO_{2(aq)}$	6.3447	$K_1 = 10^{-6.3447}$
$^{13}CO_{2(aq)}$	6.340835	$\alpha_1 = 10^{-6.340835}/10^{-6.3447}$
CO_3^{2-}	10.3288	$K_2 = 10^{-10.3288}$
$^{13}CO_3^{2-}$	10.328969	$\alpha_2 = 10^{-10.328969}/10^{-10.3288}$
$CO_{2(g)}$	−7.8136	
$^{13}CO_{2(g)}$	−7.8101825	

$$CO_3^{2-} = \frac{DIC}{\frac{[H^+]^2}{K_1K_2} + \frac{[H^+]}{K_2} + 1} \quad (4)$$

$$HCO_3^- = \frac{[H^+][CO_3^{2-}]}{K_2} \quad (5)$$

$$CO_{2(aq)} = \frac{[H^+]^2[CO_3^{2-}]}{K_1K_2} \quad (6)$$

where all parameter values are given in Table2. The associated rare isotope values can be similarly calculated from the appropriate values independently, or through a coupled solution as given in Criss [4] and many others. This independent check offers a simple means of validating all numerical model output against a basic solution before proceeding to more complex scenarios.

4.2 Component problem set 2: Radiocarbon decay with appropriate associated stable carbon isotope correction factor

Part 2 extends the inorganic carbon system simulated in the previous step to include14C. Total DIC is now divided into three isotopic components,^{14}C DIC,^{13}C DIC, and ^{12}C DIC subcomponents, resulting in explicit tracking of the$\Delta^{14}C$ and $\delta^{13}C$ values. The initial radiocarbon content is set to $\Delta^{14}C = -66‰$ following Eqs.2–3, which is effectively a modern value [26]. While the $\delta^{13}C$ of total DIC will not shift, the speciated DIC components (CO_2(aq),HCO_3^-,and CO_3^-) will all reflect unique $\delta^{13}C$ values as in the previous exercise. The key demonstration of this step is that mass-dependent radio carbon partitioning between pools is accurately simulated such that the $\Delta^{14}C$ of DIC (corrected for mass-dependent fractionation, Eqs.2and3) (1) ages with time and (2) remains consistent in all speciated and total DIC pools regardless of shifts in $\delta^{13}C$.

4.2.1 Flow and transport model specification

There is no open system behavior included in part 2 and thus no flow model is implemented. The domain is effectively 0D. In contrast to part 1, time stepping is included to track the progression of radiocarbon decay.

4.2.2 Reaction network specification

The simulations are built off of the parameters indicated in part 1 (Tables1and2) with the addition of 14C. The primary species $H^{14}CO3-$is implemented with an initial concentration of 5.65108E−13 mM and secondary species $^{14}CO2(aq)$ and$14CO_32-$are added with equilibrium constants equal to twice those given for the13C species above (Table2). This means that all mass-dependent partitioningexertedonthe13C species relative to the common12Cisalso imparted on the ^{14}C values. In addition, a simple first order homogeneous(aqueous) kinetic reaction of the form rate = constant ×activity is added in order to accommodate radioactive de-cay of ^{14}C. In this case, the rate constant is the half-life(λ) and the expression for the radiocarbon bearing total inorganic carbon concentration at any point in time (t)relative to an initial value (init) is:

$$\mathrm{Tot\_H^{14}CO_3^-} = \mathrm{Tot\_H^{14}CO_3^-}_{\mathrm{init}} \times \exp.(-\lambda t) \qquad (7)$$

With appropriate half-life of 5730 years, which equates to a rate constant of 1.209628644E−4mol/kg-H2O/year. The stoichiometry of the reaction is set such that decay of 1 mol of H14CO3−generates 1 mol of NO3−. For the current simulation, this choice of product is somewhat arbitrary, but is intended to reflect the fact that14C decays to nitrogen and thus a nitrogen bearing species is used. Therefore, a low initial NO3−value is added to the primary species list in order to facilitate this reaction.

4.2.3 Runtime parameters

The simulation is run over a duration of 10,000 years and a timeseries is recovered for the batch system allowing the user to track the radioactive decay of radiocarbon with corresponding stable isotope corrections through time. The critical aspect of this component of the benchmark is the demonstration that implementing the same mass-dependent fractionation for both ^{13}C and ^{14}C and then following the correction indicated in Eqs.2–3results in a decay curve that has correctly removed the influence of any mass-dependent differences among the species.

4.3 Component problem set 3:Simulation of natural carbon isotope ratios including kinetic fractionation in (a) a 0D batch reaction and (b) across a 1D flow path, including speciation, kinetically limited redox and biogenic mineral formation

This component introduces mass-dependent isotope fractionation in the transformation of DOC to DIC through oxidation. This kinetic reactive pathway is included in addition to the equilibrium isotopic partitioning of DIC species, resulting in a shift in the net DOC and DIC $\delta^{13}C$ pools with time in the batch reaction (part 3a) and in space across a 1D column (part3b). The principal metrics of success for this stage of the benchmark are (1) that stable isotope partitioning is correctly and reproducibly generated as a function of reaction progress (length and time) in the model. Part (a) is principally in tended to verify that the combination of kinetic and equilibrium fractionation factors is functional, followed by the addition of open system transport subject to both initial and boundary conditions in part (b).

4.3.1 Transport model specification There is no transport in part 3a. In 3b, the upgradient boundary condition is fixed to a constant inlet flow velocity of12.657 cm day−1. Dispersivity is set to 4.0 cm and the diffusion coefficient for all aqueous species is 0.919 ×10−5cm2s−1. Clearly, the use of a single diffusion coefficient for all species is not strictly accurate, but the flow rate is sufficiently fast that the system is not diffusion dominated. In this particular context, a Peclet number on the order of 1600 is obtained for the whole column. These values are loosely based on a prior reactive transport simulation and as-sociated injection of organic acid to promote redox activity in a flow-through column experiment [9,10].

4.3.2 Reaction network specification

The concentrations of aqueous species in the initial condition and influent flux are given in Table3. Part 3a uses the influent condition as indicated in the table as the initial condition in order to start with acetate in the system; part 3b uses the true initial condition listed and maintains a constant influent boundary condition thereafter. Initial solid phases are prescribed to a simplified representation of the composition of sediment in the column sourced from the Old Rifle aquifer (Table4). Redox reactions (Table5) are added individually for the two (or more) isotopes of carbon. Critically, in these simulations we make no distinction between the placement of the rare isotope within the acetate molecule, and thus no differentiation between acetate isotopomers is treated. This could be added, should interest arise, through the definition of up to

Table 3 Initial and influent concentrations of the primary aqueous species at 25 °C for part 3

Primary species	Initial concentration (mmol/kg H_2O)	Influent concentration (mmol/kg H_2O)
pH	7.2	7.2
Fe^{2+}	1.0E−08	1.0E−08
Fe^{3+}	equilib. with $Fe(OH)_{3(s)}$	equilib. with $Fe(OH)_{3(s)}$
$SiO_{2(aq)}$	0.35	0.35
Na^+	10.6	22.0
Ca^{2+}	4.47	5.28
Mg^{2+}	4.4	4.34
SO_4^{2-}	9.191	9.191
Cl^-	3.00	3.00
$CO_{2(aq)}$	8.66	10.28
Acetate	0.00	9.70
$H_2S_{(aq)}$	1.0E−15	1.0E−15
$O_{2(aq)}$	15.6E−3	15.6E−3
NH_4^+	1.5	1.5
Br^-	0.0	1.32

four distinct acetate compounds, one including only the common ^{12}C, two including one ^{13}C substitution in each of the possible locations, and a final doubly substituted species. This may be particularly relevant to those interested in carbon isotope fractionation of acetate in methanogenetic conditions [3].The associated homogeneous (aqueous) kinetic reactions are thus second order with dependence on the activity of both sulfate and acetate using appropriate rate constants (Table5)and follow the general form of rate = constant × activities of dependencies. Heterogeneous reactions are also necessary to describe the generation of elemental sulfur and precipitation of secondary minerals. Table6lists the minerals included in the simulation along with their stoichiometry, rate constants and equilibrium constants at 25 °C. Table7 contains secondary aqueous species included in the simulation with stoichiometry and equilibrium constants.

5 Results and discussion5.1 Part 1

The comparison of model output for benchmark part 1 is presented both for the distribution of aqueous species concentrations (Fig.1a) and the corresponding stable $\delta^{13}C$ isotope ratios (Fig.1b). The total concentration of the primary species, or total inorganic carbon, is always a fixed value of 5.1425 mM and the corresponding $\delta^{13}C$is + 0.9685‰. As illustrated, all models maintain this

Table 4 Initial solid phases present and allowed to form, for part 3

Mineral	Initial volume fraction (m^3/m^3)	Surface area
Goethite	3.63–4	55.2 m^2/g
$Fe(OH)_3$	9.4E−4	1.0 m^2/m^3
Quartz	0.63	1.0 m^2/m^3
FeS(am)	0.0	1.0 m^2/m^{3*}
S^0	0.0	1.0 m^2/m^{3*}

*Initial bulk surface area used to calculate precipitation of secondary sulfides

fixed concentration and isotope ratio of the primary species across the full range of pH values. In comparison to the total concentration, the individual species vary substantially as a function of pH, in close agreement with the analytical solution. The distribution favors CO2(aq) at low pH values, switching to primarilyHCO3−at neutral values, and CO_3^{2-}under basic conditions. The resulting stable isotope ratios reflect a similar mass balance, in which the $\delta^{13}C$ of CO2(aq) is effectively equivalent to the total primary species value when CO2(aq) makes up the majority of the concentration. The $\delta^{13}C$ values also agree closely with the analytical solution though slight deviations are noted for species that become extremely low in concentration as a result of rounding errors and the sensitivity of the isotopes. We further note that all concentrations reported here utilizeastandard Debye–Huckel activity model. While this may present some difficulty for benchmarking of future codes which utilize different activity models, for the present purpose, we note that there should be no difference in the corresponding isotope ratios based on either molar concentration or activity in any simulations of this type. All codes used in these simulations employ an activity model within the speciation calculation.

5.2 Part 2

The comparison of model output for benchmark part 2 is presented first as a comparison of the radiocarbon values as a function of time for the total inorganic carbon and the

Table 5 Aqueous reactions for Part 3, associated rate constants and dependencies, where * indicates the corresponding isotopologue of $C_2H_3O_2^-$

Redox reactions		k	*Dependencies*	
			SO_4^{2-}	$*C_2H_3O_2^-$
(i)	$SO_4^{2-} + {}^{12}C_2H_3O_2^- + 2\,H^+ \rightarrow +2\,{}^{12}CO_{2(aq)} + 2\,H_2O + H_2S_{(aq)}$	2000 (mol/kg-H_2O/year)	1.0	1.0
(ii)	$SO_4^{2-} + {}^{13}C_2H_3O_2^- + 2\,H^+ \rightarrow +2\,{}^{13}CO_{2(aq)} + 2\,H_2O + H_2S_{(aq)}$	1980 (mol/kg-H_2O/year)	1.0	1.0

speciated individual values through time using the CrunchTope output (Fig.2a). The critical point we wish to emphasize here is that both

the14Cand13Cisotopesofcarbon are subjected to the same mass-dependent fractionation factors which cause differences in the $\delta^{13}C$ of the species illustrated in part 1 (Fig.1b). However, applying the equations presented earlier (Eqs.2and3), we recover a $\Delta^{14}C$ value that has been corrected for this mass-dependent difference among species, and removed from the resulting ratio. This is the standard method by which radio carbon values are measured and reported by accelerator mass spectrometry facilities (see Section3), and thus, it is critical the reactive transport framework is able to accurately produce the same consistent behavior between the three-isotope system. Furthermore, the decay curve due to radioactivity reproduces the correct decrease in $\Delta^{14}C$, as implemented in Eq. 7 (see Section3).The second demonstration uses an arbitrary choice of car-bon species since the radiocarbon notation renormalizes all species to the same value as a result of the correction for mass-dependent fractionation. For any carbon species, the four software packages tested showed excellent agreement in both the half-life of radiocarbon and the associated treatment of mass-dependent partitioning.

5.3 Part 3

The final aspect of the benchmark is divided into two components. First, part 3a presents a 0D batch reaction in which anorganic carbon (acetate) is oxidized to inorganic carbon (TIC)coupled with the reduction of sulfate to sulfide. Next, part 3 bimplements this simulation in a 1-m-long advective flow field based on the column study reported by Druhan et al. [9].

5.3.1Part3 a

The first aspect of part 3 allows us to introduce several additional reactive and fractionating pathways in a closed system to check the accuracy of the kinetic oxidation of acetate prior to opening the system to flow and transport. Notably, in this part 3a, the redox reaction has a first order dependence on both the total acetate and total sulfate concentration, and is thus second order overall. The 1:1

Table 6 Heterogeneous reactions for part 3

Mineral	log K_{eq}	log k (mol/m^2/s)	H+	Stoichio Fe++	Coeff Fe+++	H2S(aq)	CO2(aq)	SiO_2(aq)
Goethite	0.5345	−35	−3	0	1	0	0	0
$Fe(OH)_3$	4.300	−3	−3	0	1	0	0	0
Quartz	−3.9993	−35	−1	1	0	0	0	1
$FeS_{(am)}$	3.500	−3	−2	1	0	1	0	0
S^0	−21.1304	−3	−2	−2	2	1	0	0

Table 7 Homogenous reactions for part 3

Species	log K	H+	Stoichiometric coefficient			Ca++	Mg++	Cl-	SO4--	H2S(aq	CO2(aq)	Acetat	SiO2(a	O2(aq)	NH4+	Br-
			Fe++	Fe+++	Na+											
OH-	1.40E+01	−1	0	0	0	0	0	0	0	0	0	0	0	0	0	0
HCO3-	6.34E+00	−1	0	0	0	0	0	0	0	0	1	0	0	0	0	0
CO3--	1.67E+01	−2	0	0	0	0	0	0	0	0	1	0	0	0	0	0
FeOH+	9.50E+00	−1	1	0	0	0	0	0	0	0	0	0	0	0	0	0
FeS(aq)	9.20E+00	−2	1	0	0	0	0	0	0	1	0	0	0	0	0	0
FeCO3(aq)	1.19E+01	−2	1	0	0	0	0	0	0	0	1	0	0	0	0	0
CaOH+	1.29E+01	−1	0	0	0	1	0	0	0	0	0	0	0	0	0	0
CaCO3(aq)	1.34E+01	−2	0	0	0	1	0	0	0	0	1	0	0	0	0	0
CaSO4(aq)	−2.10E+00	0	0	0	0	1	0	0	1	0	0	0	0	0	0	0
CaHCO3+	5.30E+00	−1	0	0	0	1	0	0	0	0	1	0	0	0	0	0
MgCO3(aq)	1.37E+01	−2	0	0	0	0	1	0	0	0	1	0	0	0	0	0
MgSO4(aq)	−2.41E+00	0	0	0	0	0	1	0	1	0	0	0	0	0	0	0
Acetic_acid	−4.75E+00	1	0	0	0	0	0	0	0	0	0	1	0	0	0	0
HS-	6.98E+00	−1	0	0	0	0	0	0	0	1	0	0	0	0	0	0
S--	1.99E+01	−2	0	0	0	0	0	0	0	1	0	0	0	0	0	0

decrease in acetate and sulfate (Fig.3a) reflects their mole for mole stoichiometry in the redox reaction. The TIC concentration correspondingly increases as a result of acetate oxidation, and the sulfide concentration also includes a source due to sulfate reduction; however, the presence of Fe(II) rapidly precipitates any sulfide present as FeS and thus the concentration remains very low throughout the simulation. The corresponding kinetic isotope fractionation factor which enriches the $\delta^{13}C$ of the residual acetate pool in the rare isotope is 0.99 (10‰). It is important to note that this value is quite large for oxidation of organic matter, which is typically on the order of 0.999 (1‰) in most natural settings [3,12,17,30]. The present study utilizes acetate, a low molecular weight dissolved species, which may support a higher value, but primarily, we implement 10‰simply for illustrative purposes to create a large shift in the isotopes which is easy to observe. Those adjusting this benchmark set to specific applications are advised to carefully constrain the fractionation factors appropriate to their system. In the residual acetate pool, the increase in $\delta^{13}C$ appears effectively linear as the corresponding drop in concentration (Fig.3a) is relatively small. The more classic distillation type behavior becomes evident if the results are plotted as $\delta^{13}C$ vs. 1/[acetate] as in the classic Rayleigh model. The effect of this enrichment is evident both in the increase in $\delta^{13}C$ of acetate through time (Fig.3b) as well as the corresponding decrease in $\delta^{13}C$ of TIC, which is preferentially receiving ^{12}C carbon relative to ^{13}C carbon as a result of this minor difference in rates. The isotopic values of acetate and TIC are not perfect mirror images of one another, due to the fact that there was TIC in the initial condition and thus the $\delta^{13}C$ signature imparted by acetate oxidation is reflected as a function of mass balance with the original TIC present in the system.

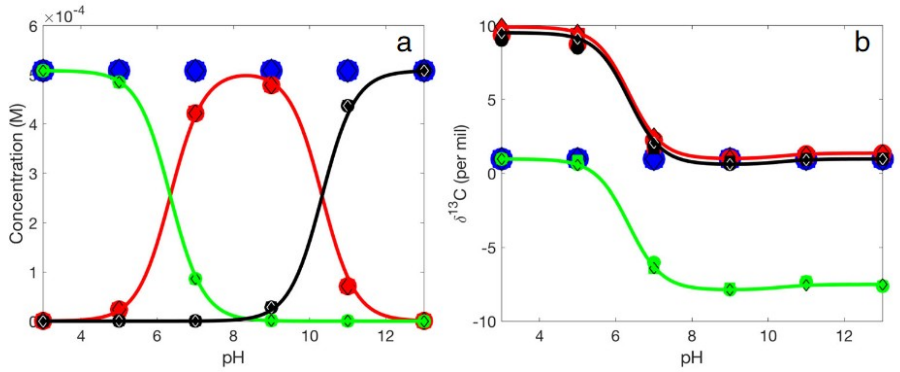

Fig. 1 Model comparison of total inorganic carbon (blue), speciated $CO_2(aq)$ (green), HCO_3^- (red), and CO_3^{2-} (black) including analytical solutions illustrated as continuous lines, and symbols representing simulation values for CrunchTope (squares), ToughReact (circles), GWB (triangles), and Hytec (diamonds). **a** Concentrations and **b** stable isotope ratios. Data points generally overlap and are often indistinguishable in the figures

signature imparted by acetate oxidation is reflected as a function of mass balance with the original TIC present in the system.

5.3.2Part3b

The final component of the benchmark places the simulation developed in part 3a into a 1D flow field with an initial condition (Table3) that includes no acetate. The upgradient boundary condition is then fixed to ahigh-acetate concentration, and the organic acid subsequently advects down gradient and establishes a steady-state concentration profile in which both acetate(Fig.4a) and sulfate concentrations decrease with distance. Though not illustrated here, this aspect of the benchmark may be used to test both the steady-state concentration profiles, as well as the transient approach

to these steady-state values from the initial condition. Generally, the major ion concentrations reach steady values at the effluent end of the domain in approximately 10 days. A 1:1 decrease in acetate and sulfate is again noted as in part 3a, and again, the sulfide concentrations remain low as a result of secondary mineral formation. The stable carbon isotope ratios for acetate (Fig.4b) enrich again as a result of the fractionation factor of 0.99and all simulations show excellent agreement. Again, the increase in isotope ratio appears linear when plotted as a function of distance, and the more classic distillation type behavior would be clear if one chooses to replot $\delta^{13}C$ vs.1/[acetate] as in the classic Rayleigh model. The corresponding inorganic carbon is here illustrated as speciated HCO3−rather than TIC, and again demonstrates a balance between influent inorganic ccarbon and the oxidation of

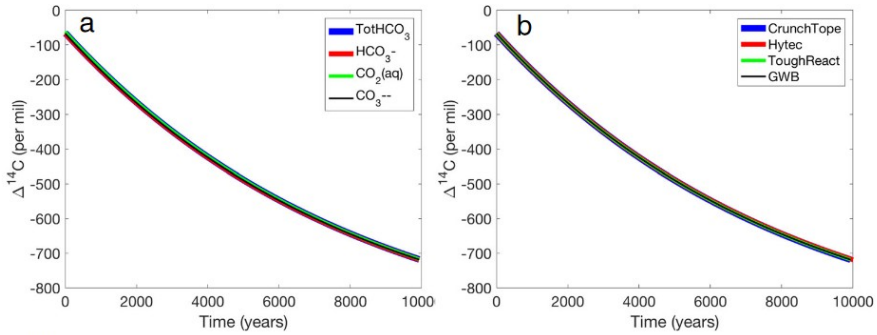

Fig. 2 Normalized $\Delta^{14}C$ values reported using Eqs. 2, 3, and 7 with embedded mass-dependent fractionation correction. **a** CrunchTope output for the total inorganic carbon (blue), speciated CO_2(aq) (green), HCO_3^- (red), and CO_3^{2-} (black) illustrating the radiocarbon decay curve through time after appropriate stable isotope ratio correction. **b** Comparison between models using an arbitrary choice of species, illustrating CrunchTope (blue), Hytec (red), ToughReact (green), and GWB (black)

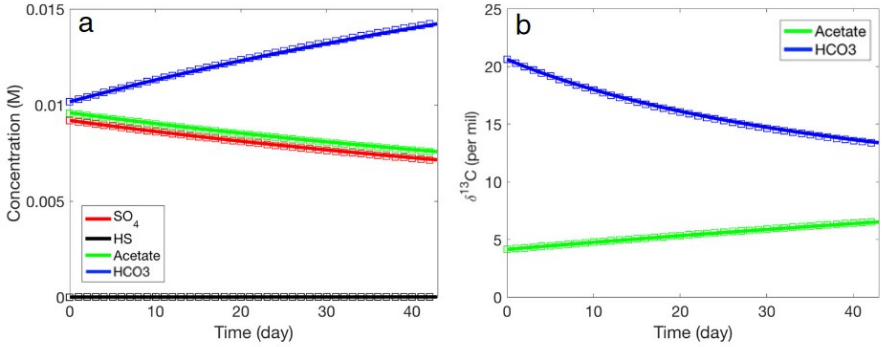

Fig. 3 A batch reaction including a kinetic redox transformation converting acetate (green) to inorganic carbon (blue) coupled to the reduction of sulfate (red) to sulfide (black). This simulation is run over 43 consecutive days and includes all equilibrium fractionations among carbon species as well as a kinetic fractionation associated with acetate oxidation. Solid lines encompass the simulations of both CrunchTope and ToughReact. The hollow symbols overlaid on each line are the Hytec output. **a** Concentrations and **b** carbon isotope ratios

acetate as a function of flow and reaction rate. For illustrative purposes, a second simulation is included using CrunchTope in which the kinetic fractionation factor for acetate oxidation has been set to 1.0 (Fig.4b). Under this condition, the acetate isotope ratio remains constant, but the speciated HCO3−stable isotope ratio still shifts over the length of the column as a result of the equilibrium fractionation associated with changes in pH along the flow path.

6Summary

Carbon isotopes partition as a result of both mass-dependent fractionation pathways, and in the case of ^{14}C, through radioactive decay. Though14C is not immune to mass-dependent effects, the standard method of reporting this value removes such influences through correction with the corresponding $\delta^{13}C$ value. Though com-mon practice, this coupled behavior has never been systematically benchmarked in a reactive transport frame-work. More broadly, this benchmark is the first to provide a validated and sequential means of testing models for multiple isotopes in which the same isotope system is present across multiple coexisting species (CO2(aq),HCO3−,CO32−) with distinct partitioning. Both batchand flow-

through examples indicate agreement across four widely used software platforms, and future model development for such multi-isotope applications may use this as a basis for validation.

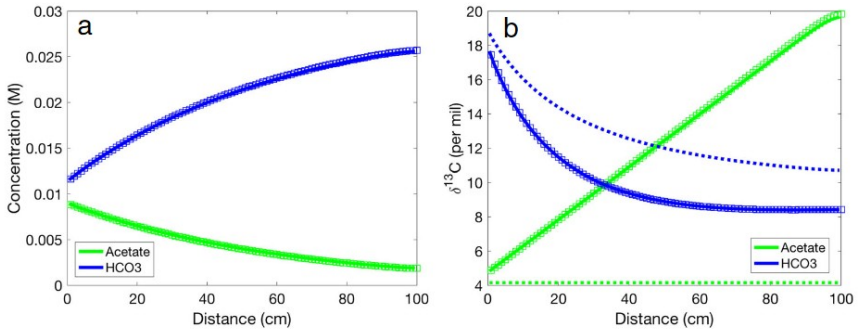

Fig. 4 A 1D flow field 100 cm in length plotted 43 days after the start of the simulation. At this period in time, all solutes have reached steady-state profiles across the domain. The reactions taking place are comparable to those introduced in part 3a and include all prior equilibrium fractionation among carbon species as well as a kinetic fractionation associated with acetate oxidation. Solid lines encompass the simulations of both CrunchTope and ToughReact. The hollow symbols overlaid on each line are the Hytec output. **a** Concentrations and **b** carbon isotope ratios. For illustrative purposes, a second simulation is shown from CrunchTope output in **b** in which the kinetic fractionation factor for carbon isotopes during oxidation has been changed to 1.0 (dashed lines)

References

1. Arora, B., ??engör, S.S., Spycher, N.F., & Steefel, C.I.: A reactive transport benchmark on heavy metal cycling in lake sediments. Comput. Geosci.19(3), 613–633 (2015)

2. Arora, B., Davis, J.A., Spycher, N.F., Dong, W., & Wainwright,H.M.: Comparison of electrostatic and non-electrostatic models for U (VI) sorption on aquifer sediments. Groundwater.56(1),73–86 (2018)

3. Conrad, R., Klose, M., Yuan, Q., Lu, Y., Chidthaisong, A.: Stable carbon isotope fractionation, carbon flux partitioning and priming effects in anoxic soils during methanogenic degredation of strawand soil organic matter. Soil Biol. Biochem.49,193–199 (2012)

4. Criss, R.E.: Principles of stable isotope distribution. Oxford University Press, New York (1999)

5. Dale, A.W., Bruchert, V., Alperin, M., Regnier, P.: An integrated sulfur isotope model for Namibian shelf sediments. Geochim.Cosmochim. Acta.73,1924–1944 (2009).https://doi.org/10.1016/j.gca.2008.12.015

6. Druhan, J.L., Maher, K.: A model linking stable isotope fractionatoin to water flux and transit times in heterogeneous po-rous media. Procedia Earth Planet. Sci.10,179–188 (2014)

7. Druhan, J.L., Steefel, C.I., Molins, S., Williams, K.H., Conrad,M.E., DePaolo, D.J.: Timing the onset of sulfate reduction over multiple subsurface acetate amendments by measurement and modeling of sulfur isotope fractionation. Environ. Sci. Technol.46,8895–8902 (2012).https://doi.org/10.1021/es302016p

8. Druhan, J.L., Steefel, C.I., Williams, K.H., DePaolo, D.J.: Calcium isotope fractionation in groundwater: molecular scale processes influencing field scale behavior. Geochim. Cosmochim. Acta.119,93–116 (2013)

9. Druhan, J.L., Steefel, C.I., Conrad, M.E., DePaolo, D.J.: A large column analog experiment of stable isotope variations during reactive transport: I. A comprehensive model of sulfur cycling and deltaS-34 fractionation. Geochim. Cosmochim. Acta.124, 366–393(2014a).https://doi.org/10.1016/j.gca.2013.08.037

10. Druhan, J.L., Bill, M., Lim, H., Wu, C., Conrad, M.E., Williams,K.H., DePaolo, D.J., Brodie, E.L.: A large column analog experiment of stable isotope variations during reactive transport: II.Carbon mass balance, microbial community structure and predation. Geochim. Cosmochim. Acta.124,394–409 (2014b)

11. Eckert, D., Rolle, M., Cirpka, O.A.: Numerical simulation of iso-tope fractionation in steady-state bioreactive transport controlled bytransverse mixing. J. Contam. Hydrol.140,95–106 (2012).https://doi.org/10.1016/j.jconhyd.2012.08.010

12. Fey, A., Claus, P., Conrad, R.: Temporal change of 13C-isotopesignatures and methanogenic pathways in rice field soil incubated anoxically at different temperatures. Geochim. Cosmochim. Acta.68(2), 293–306 (2004)

13. Gibson, B.D., Amos, R.T., Blowes, D.W.: S-34/S-32 Fractionation during sulfate reduction in groundwater treatment systems: reactive transport modeling. Environ. Sci. Technol.45,2863–2870 (2011).https://doi.org/10.1021/es1038276

14. Hubbard, C.G., Cheng, Y., Engelbrekston, A., Druhan, J.L., Li, L.,Ajo-Franklin, J.B., Conrad, M.E.: Isotopic insights into microbial sulfur cycling in oil reservoirs. Front. Microbiol.5, 480 (2014)

15. Hunkeler, D., Van Breukelen, B.M., Elsner, M.: Modeling chlorine isotope trends during sequential transformation of chlorinated eth-enes. Environ. Sci. Technol.43,6750–6756 (2009).https://doi.org/10.1021/es900579z

16. Jamieson-Hanes, J.H., Amos, R.T., Blowes, D.W.: Reactive trans-port modeling of chromium isotope fractionation during Cr(VI)reduction. Environ. Sci. Technol.46,13311–13316 (2012).https://doi.org/10.1021/es3046235

17. Lapham, L., Proctor, L., Chanton, J.: Using respiration rates andstable carbon isotopes to monitor the biodegradation of Orimulsion by marine benthic bacterial. Environ. Sci. Technol.33(12), 2035–2039 (1999)

18. Lee, M.K., Bethke, C.M.: A model of isotope fractionation in reacting geochemical systems. Am. J. Sci.296(9), (1996)

19. Li, L., Maher, K., Navarre-Sitchler, A., Druhan, J.L., Meile, C.,Lawrence, C., Moore, J., Perdrial, J., Sullivan, P., Thompson, A.,Jin, L., Bolton, E.W., Brantley, S.L., Dietrich, W., Mayer, K.U.,Steefel, C.I., Valocci, A., Zachara, J., Kocar, B.,

Mcintoch, J.,Bao, C., Tutolo, B.M., Beisman, J., Kumar, M., Sonnenthal, E.:Expanding the role of reactive transport models in critical zone processes. Earth Sci. Rev.165,280–301 (2017)

20. Maher, K., Steefel, C.I., DePaolo, D.J., Viani, B.E.: The mineral dissolution rate conundrum: insights from reactive transport model-ing of U isotopes and pore fluid chemistry in marine sediments. Geochim. Cosmochim. Acta.70, 337–363 (2006a).https://doi.org/10.1016/j.gca.2005.09.001

21. Maher, K., DePaolo, D.J., Christensen, J.N.: U-Sr isotopic speed-ometer: fluid flow and chemical weathering rates in aquifers.Geochim. Cosmochim. Acta.70,4417–4435 (2006b).https://doi.org/10.1016/j.gca.2006.06.1559

22. Mook, W.G.:13C in atmospheric CO2. Neth. J. Sea Res.20,211–223 (1986)

23. Rolle, M., Chiogna, G., Bauer, R., Griebler, C., Grathwohl, P.:Isotopic fractionation by transverse dispersion: flow-though micro-cosms and reactive transport modeling study. Environ. Sci.Technol.44,6167–6173 (2010).https://doi.org/10.1021/es101179f

24. Steefel, C.I., Druhan, J.L., Maher, K.: Relationships between transit time of water and the fluxes of weathered elements through the critical zone. Procedia Earth Planet. Sci.10,16–22 (2014)

25. Steefel, C.I., Appelo, C.A.J., Arora, B., Jacques, D., Kalbacher, T.,Kolditz, O., Lagneau, V., Lichtner, P.C., Mayer, K.U., Meeussen,J.C.L., Molins, S., Moulton, D., Shao, H.,Šimunek, J., Spycher, N.,Yabusaki, S.B., Yeh, G.T.: Reactive transport codes for subsurface environmental simulation. Comput. Geosci.19(3), 445–478 (2015)

26. Trumbore, S.: Radiocarbon and soil carbon dynamics. Annu. Rev.Earth Planet. Sci.37,47–66 (2009).https://doi.org/10.1146/annurev.earth.36.031207.124300

27. Van Breukelen, B.M., Rolle, M.: Transverse hydrodynamic dispersion effects on isotope signals in groundwater chlorinated solvents' plumes. Environ. Sci. Technol.46,7700–7708 (2012).https://doi.org/10.1021/es301058z

28. van der Lee, J., De Windt, L., Lagneau, V., Goblet, P.: Module-oriented modeling of reactive transport with HYTEC. Comput.Geosci.29,265–275 (2003)

29. Wanner,C.,Druhan,J.L.,Amos,R.T.,Alt-Epping,P.,Steefel,C.I.:Benchmarking the simulation of Cr isotope fractionation. Comput. Geosci. (2015).https://doi.org/10.1007/s10596-014-9436-9

30. Werth, M., Kuzyakov, Y.:13C-fractionation at the root-microorganisms-soil interface: a review and outlook for partitioning studies. Soil Biol. Biochem.42,1372–1384 (2010